SESSION C

Wednesday, October 21, 1992

8:30 a.m.

Applications

Papers:

1. Recent Developments in Monte Carlo Techniques
   - George Zimmerman (LLNL)

2. Simulation of Particle Beam Diodes with an Electromagnetic Particle-in-Code
   - Jeff Quintenz (SNL)

3 Monte Carlo Laboratory Status in VNIEF
   - Yuriy Kochubey (Arzamas)

4. Radiation Transport Calculation without Local Thermodynamic Equilibrium
   - Yuriy Kochubey (Arzamas)

5. Mathematical Modeling of Flexible Plastics and Destruction of Materials. Seismic Decoupling of an Underground Nuclear Explosion
   - Vladimir Bychendov, Valentin Kuropatenko, et al (Chelyabinsk)

SESSION C

Applications

RECENT DEVELOPMENTS IN MONTE CARLO TECHNIQUES

G. B. ZIMMERMAN
Lawrence Livermore National Laboratory
Livermore, California

ABSTRACT

Many aspects of the using Monte Carlo methods to transport particles in complex geometries are explored. The thermonuclear source of particles is presented as a Monte Carlo simulation of the reaction process. Corrections due to both bulk and thermal Doppler motion are described as are detailed general purpose formulas for the stopping of charged particles. In heterogeneous materials characterized by binary Markovian statistics models are presented for the effects on both thermal and Monte Carlo transport. It is found that the effects of angular Coulomb scattering must be included in models of charged particle transport through heterogeneous materials.

SESSION C

Applications

SIMULATION OF PARTICLE BEAM DIODES WITH AN ELECTROMAGNETIC PARTICLE-IN-CODE

Application of the QUICKSILVER 3-D electromagnetic particle-in-cell code for the simulation of intense particle beam diodes and pulsed power devices

J. P. Quintenz, R. S. Coats, M. P. Desjarlais, M. L. Kiefer,
T. D. Pointon, D. B. Seidel, S. A. Slutz

Pulsed Power Sciences Directorate, 1200
Sandia National Laboratories, Albuquerque, NM 87185 USA

Abstract

The QUICKSILVER[1] code was originally developed at Sandia National Laboratories for use in research in the Pulsed Power Sciences Directorate. QUICKSILVER is a three-dimensional, electromagnetic particle-in-cell code that can be used to simulate a wide variety of pulsed power devices. QUICKSILVER has been used to aid research in various pulsed power programs including: new accelerator concept development, light ion inertial confinement fusion, weapons effects simulation and microwave device development. The QUICKSILVER suite of codes consists of a user input interface called MERCURY that interactively preprocesses input to help the user define the simulation. MERCURY resides on a variety of workstation platforms. QUICKSILVER is the workhorse code that performs the simulation and is targeted for CRAY class computers. There are several different postprocessors for the suite for performing one-, two-, and three-dimensional data rendering and manipulation.

This talk will highlight the application of the QUICKSILVER suite to simulation of intense ion diodes used in Sandia's light ion fusion program. These simulations have illuminated the physics of these devices and have led to solutions to the problem of beam divergence due to electromagnetic instabilities[2].

1 D. B. Seidel, M. L. Kiefer, R. S. Coats, T. D. Pointon, J. P. Quintenz, and W. A. Johnson, in *Computational Physics*, edited by A. Tenner (World Scientific, Singapore), 475 (1991).

2 M. P. Desjarlais, T. D. Pointon, D. B. Seidel, R. S. Coats, M. L. Kiefer, J. P. Quintenz and S. A. Slutz, Phys. Rev. Lett. 35, 3094 (1991).

SESSION C

Applications

MONTE CARLO LABORATORY STATUS IN VNIIEF

E.N.Donskoy, V.A.Eltsov, A.K.Zhitnik, N.V.Ivanov,
Yu.K.Kochubey, A.I.Morenko, L.Z.Morenko, V.I.Roslov,
A.B.Ronzhin, A.N.Subbotin

This reports contains some data on the Monte Carlo laboratory. Production codes and methods used are briefly decribed.

MONTE CARLO LABORATORY STATUS IN VNIIEF

E.N.Donskoy, V.A.Eltsov, A.K.Zhitnik, N.V.Ivanov,
Yu.K.Kochubey, A.I.Morenko, L.Z.Morenko, V.I.Roslov,
A.B.Ronzhin, A.N.Subbotin

The Monte Carlo Laboratory was founded in the VNIIEF Computational Center in 1958. The major objectives assigned to the laboratory consisted of critical parameter and neutron transport calculations. These calculations are still considered the main ones in the Laboratory. The Laboratory has a variety of programs which are used to run 600 - 700 applications per month. The main programs are represented by:

S-90 - calculates coupled neutron-photon transport, activation and critical parameters;

ELIZA - calculates coupled electron, positron and photon transport.

Typical problem geometry calculated with above programs is represented by 2-dimensional axisimmetric system which is composed of regions bounded by second-degree surfaces. Algorithm to control such geometry was developed in 1968. S-90 control algoritms provide completely "half-free" execution when specifying 2-dimensional geometry.

A geometry composed of differently oriented 2-dimensional systems and parallelepipeds can also be specified. Moreover, general three-dimensional geometries consisting of second-degree surfaces though a reliable control is still a problem for such calculations.

The programs have good possibilities for specification of particle sources (volume, surface and point sources) including those beyond the system with energy and angular distributions being set.

The output can be of two types- standard and ordered. Standard results are always output and used for calculation validity control. These include unidirectional particle and energy fluxes, average source particle parameters, total and regional number of collisions and reactions, particle increase per reaction, physical and simulated particle death and some others. Collision estimator represents the main estimator for standard results.

Ordered results are requested individually for each computati-

on. This result type is essentially represeted by fluxes, doses and reaction numbers distributed over particle phase coordinates which include energy, spatial coordinates, time, collision number, generation number, particle type etc. The track-lengh estimator serves the main estimator for this output.

For initial data specification, problem-oriented languages using syntax translator which consists of two components - a loader and an analyser. The loader allows to automate the syntax rule specifications. The analyser verifies whether initial data is correct or not and generates a standard parsing tree which is operated by data generation routines.

I. S-90 CODE.

The code computes neutron-photon transport, photon generation in n-γ reactions and in activation processes.

Several libraries are used to describe data on interaction between neutron, γ-quanta and material - our own library created by G.Goncharov from VNIIEF, BAS-78 designed under the guidance A.Vasiliev from VNIITF, multigroup cross-section data calculated under the guidance G.Farafontov from VNIIEF and in some cases ENDL-82.

The code allows calculations of interactions between neutrons and material in free molecular gas model, that is material atom velocities are assumed to have Maxwell distribution with given temperature. This means that the differential frequence of collisions has the form

$$\lambda(\vec{v} \to \vec{v}') = \int P(d\vec{u})|\vec{v} - \vec{u}|\sigma(\vec{v} - \vec{u} \to \vec{v}' - \vec{u})$$

where $P(d\vec{u})$ is Maxwell distribution and $\sigma(\vec{v} \to \vec{v}')$ is differential cross-section. This approximation was made standard affer an efficient method was developed for sampling collisions with such frequency.

The main methods increasing the accuracy include splitting, russian roulette and weight windows on surfaces which are the part of both original and so called governing geometry that does not relate to the former. Particle paths are modeled simultaneously in both original and governing geometries the latter having a more simple form and being used to control the computation.

Computational cost-efficiency can be simply and offten effectively increased by forcing a particle death when it enters the phase space domains which have negligible contributions to the functionals to be computed.

In 1968 V.Ogibin from VNIITF proposed the test particle method to compute the functionals in geometrically small regions. S-90 uses the following implementation of this technique.

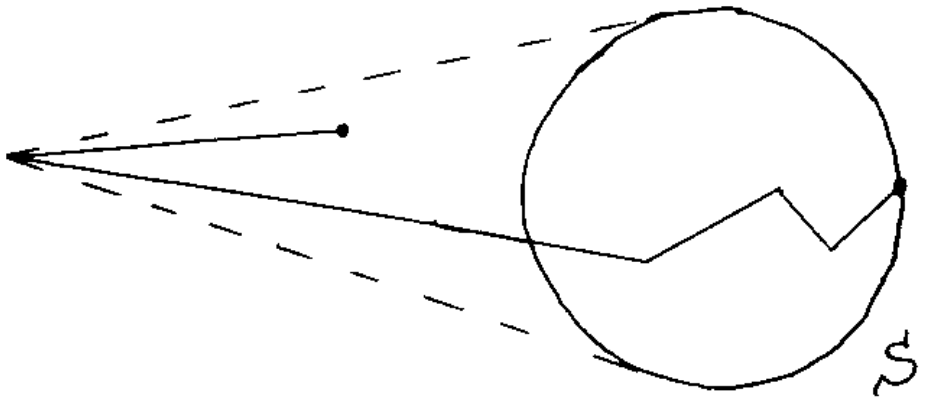

Fig. 1

A portion of the space where functionals are to be computed is surrounded with a sphere S. When a simulated (basic) particle collides beyond S, a sphere scope cone with a corresponding weight receives an emitted test particle which is simulated as follows. The particle dies when colliding beyond S, if it reaches the boundary of S, the test particle is further simulated in an usual manner and the results are registerd for it. The particle dies when crossing the boundary of S. No results is registered for basic particle.

Functionals can be computed using test particles which are in turn generated by other test particles. Consider an example of such approach.

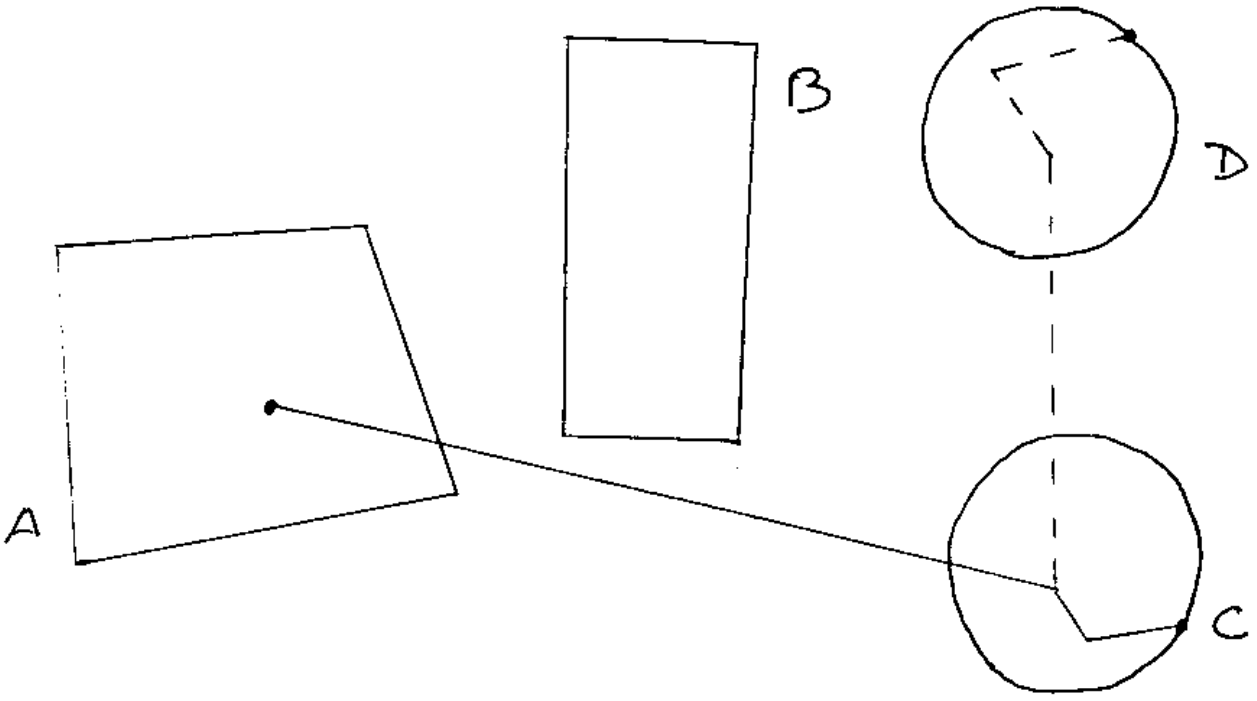

Fig. 2

Particles are generated in region A, and results are to be computed in region D which is shielded from A by an absorber layer B. The major contribution to the results is provided by particles colliding in region C. To evaluate this contribution due to collisions in regions A and B, test particles are emitted into region C, the former generating other test particles for region D.

For estimation of the flux at a point two criteria are used. The first one is either a common exponential estimator or its modification which is as follows.

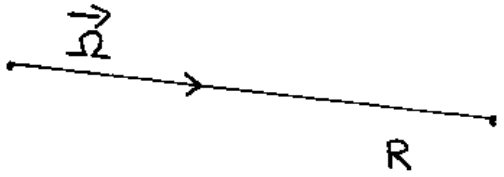

Fig. 3

Each collision point emits a test particle to the detector with the particle weight given by

$$W = \frac{p(\vec{\Omega})}{R^2}$$

where $p(\vec{\Omega})$ is the probability density for the flight to the detector. If a collision occurs prior to detector, the particle dies, otherwise a result is registered for it and the particle is out.

Another estimator, unlike the above one, has a finite variance.

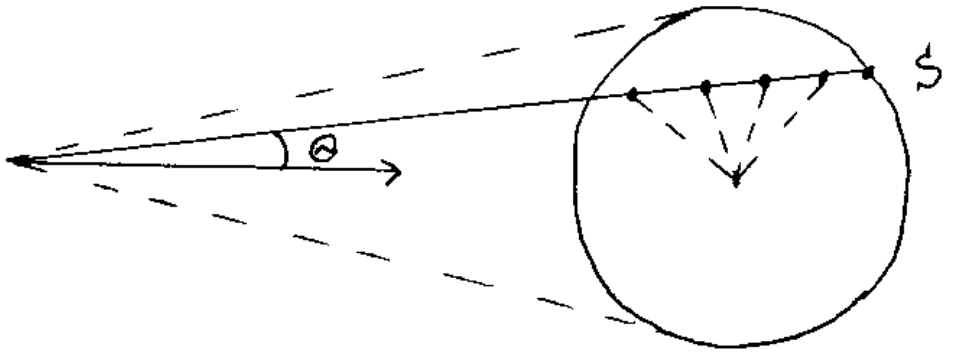

Fig. 4

The detector is surrounded with a sphere S of radius R. If the collision point is beyond S, an exponential estimator is taken for it and a test particle is emitted to the sphere scope cone with a probability proportional to the solid angle. The flight direction for this particle is chosen according to the distribution proportional to $\cos\frac{\theta}{2}$ where θ is angle between the flight direction and the direction to the detector. Biase of flight direction distributions accounted by the weight assigned to the particle. If the collision occurs prior to S, the particle dies otherwise it continues moving inside the sphere with collision cross-section $\Sigma R/r \geq \Sigma$. An exponential estimator with the weight r/R is applied from each collision point to evaluate the flux. The particle dies when the real collision occurs for the first time or S is reached.

If the collision point is inside S, it emits a test particle which is modeled with the previous algorithm.

Substantial efficiency increase for S-90 computations was obtained by the following implementation of path simulations. The energy variation range for E particles is divided into 100 inter-

vals which are uniform with respect to ln E. For each spatial region of an application, maximum cross-section within each energy interval are calculated. For simulating, cross-section are represented by calculated maximum cross-section with sampling them being highly cost-efficient, hence optically thin regions can be cost-efficiently computed. If the collision occurs inside a region the material is chosen where the collision takes place. For optimizing these computations, materials are ordered according to decreasing concentrations, so that the first materials in the computation sequence account for the highest selection probability. In the case of a fiction collision after all materials have been sampled, the total true cross-section becomes known and the next collision point is simulated using this cross-section that is zero probability of fiction collision. This algorithm prevents the number of fiction collisions from growing considerably.

2. ELIZA CODE.

This program computes coupled γ-quantum, electron and positron transport. The following γ-quanta material interaction processes are considered - noncoherent (Compton) scattering with respect electron binding in the atom, coherent (Raighley) scattering, photoabsorption with respect to the emission of fluorescent quanta and Oze-electrons, generation electron-positron pairs. For electrons and positrons, elastic scattering on the nucleus, scattering on the free electron, K-shell ionization, bremsstrahlung and two-photon annihilation of positrons are considered. The energy range varies from 1 Kev to 100 Mev.

ELIZA capabilities are very similar to those of [illegible] in view of geometry, source, result specification and γ-quanta simulating.

For charged particle calculations, one has to overcome some specific difficulties associated with special aspects of interaction between these particles and material. The most important is that Coulomb interaction dominates the interaction between charged particles and material the former being characterized by forward-extended scattering indicatrix and large cross-section. Therefore a particle experiences so many collisions that they cannot be directly simulated. Various authors proposed a number of methods to avoid this. ELIZA uses an implementation of catastrophic collision method where the differential cross-section is represented as sum of two

addends one of them describeing small angle collisions and the other the remaining type. Small angle collisions are described using Fokker-Planck approximation. A third order accuracy method is developed for step-by-step path construction to simulation diffusion traectories occuring when this approach is used.

ELIZA employs a number of methods including the above mentioned to increase the computational efficiency. It should be noted that secondary particle generation points are systematically redistributed regarding their significance. The computations are made considerable more cost-efficient by using minimum sphere method.

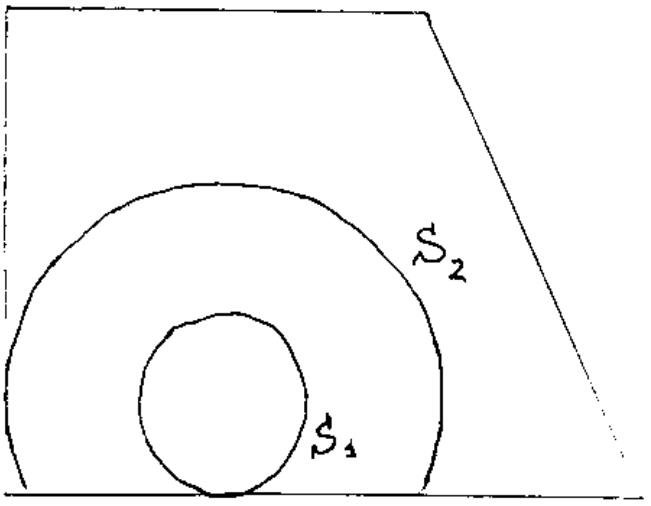

Fig. 5

For each surface limiting a region, a sphere is constructed with its center being located at the particle position and having a radius that equals the distance to that portion of the surface which is within the region boundary. Two minimum radius spheres, S_1 and S_2, are selected from the set. As long as the particle remains within S_1, its trajectory intersections with the region are not considered. If the particle location is between S_1 and S_2 trajectory intersections with one surface only are considered. If the particle crosses the region boundary or leaves S_2, the spheres are reconstructed.

3. RELATED DEVELOPMENTS.

In addition to the above, other developments are performed by the laboratory. We shall present some of them.

1. Our laboratory developed methods and programs for calculations of nonlinear neutron transport and neutron and nuclear reaction kinetics in moving media. For coupled computations of gasdynamic and other physical processes, the programs are switched to corresponding routines describing these processes which were developed by the Computational Center. Currently, the computations are performed in one- and two-dimensional geometries and do not compete with more cost-efficient difference methods regarding the mass nature of calculations. The estimates obtained from experimental computations encourage one to expect a change of situation in the three-dimensional case. Now three-dimensional method developments are under way.

Note that the need for such methods is motivated by the Monte Carlo method advantages exploited in complicated applications - introduction of other particle types (α-particles, protons, deuterons), nonequilibrium of plasma components, "exotic" scattering nuclei (both physical and modeled). While these applications are not massive, they still need to be computed on regular basis both in simple and complex geometries.

2. Parameter calculations for the electromagnetic pulse EMP produced in air by moving fast Compton electrons is one of the nonlinear problems solved by our Center. Mathematically, this problem reduces to a combined solution of the kinetic equation for electrons, Maxwell equations and equations for air ionization kinetics. Since the problem is complicated and multidimensional, the electron transport is usually calculated approximately with Longmire method. For quantitative estimation of this method, our laboratory developed a method for EMP parameter calculations in one-dimensional geometry where the electron transport is accurately computed with Monte Carlo method.

3. Because of ever growing interest to environmental applications, the laboratory designed methods to calculate area pollution from a given source of aerosole particles.

If sufficiently realistic physical approximations are made,

the problem reduces to finding aerosole concentration $n(\vec{x},t)$, $\vec{x} = (x_1,x_2,x_3)$, $x_3 \geq 0$, satisfying the diffusion equation with the diagonal diffusion tensor and drift velocity depending only on x_3 and t:

$$\frac{\partial n}{\partial t} = \mathrm{div}\vec{j} + S, \qquad j_i = D_i\frac{\partial n}{\partial x_i} - u_i n,$$

$$n(\vec{x},0) = Q(\vec{x}),$$

$$cn(x_1,x_2,0,t) - j_3(x_1,x_2,0,t) = 0.$$

Here $\vec{D} = \vec{D}(x_3,t)$ - is the diagonal diffusion tensor, $\vec{u} = \vec{u}(x_3,t)$ - is the drift velocity, $Q(\vec{x})$, $S(\vec{x},t)$ - are initial distribution and aerosole source, respectively.

When developing the method, we focussed on calculating aerosole dropout density on the underlying surface $x_3 = 0$,

$$N(x_1,x_2) = \int_0^\infty j_3(x_1,x_2,0,t)\,dt .$$

The method efficiency is obtained by eventually representing $n(\vec{x},t)$ as an integral superposition of normal distributions

$$n(\vec{x},t) = \frac{1}{\pi}\int d\vec{\alpha}d\vec{\beta}\; n(\vec{\alpha},\vec{\beta},x_3,t) \cdot$$

$$\cdot \frac{\exp\left\{-\dfrac{(x_1-\beta_1)^2}{4\alpha_1} - \dfrac{(x_2-\beta_2)^2}{4\alpha_2}\right\}}{\sqrt{\alpha_1\alpha_2}},$$

where $\vec{\alpha} = (\alpha_1,\alpha_2)$ and $\vec{\beta} = (\beta_1,\beta_2)$ - are parameters of normal distributions. By substituting this expression into the original equation one finds n to satisfy the equation

$$\frac{\partial n}{\partial t} + \frac{\partial n}{\partial x_1} - \alpha_1\frac{\partial n}{\partial x_3} = \frac{\partial^2 n}{\partial x_3^2} - n,$$

$$\hat{j} = D_3 \frac{\partial \hat{n}}{\partial x_3} - u_3 \hat{n},$$

$$c\hat{n}(\vec{\alpha},\vec{\beta},0,t) - \hat{j}\,(\vec{\alpha},\vec{\beta},0,t) = 0,$$

$$\hat{Q}(\vec{\alpha},\vec{\beta},x_3) = Q(\vec{\beta},x_3)\delta(\vec{\alpha}), \quad \hat{S}(\vec{\alpha},\vec{\beta},x_3,t) = S(\vec{\beta},x_3,t)\delta(\vec{\alpha}).$$

The particle walking determined by this equation is diffusive over x_3 only. This simplifies considerably construction of the trajectories simulated with distributions obtained from analytical solutions for one-dimensional diffusion equation with piecewise-constant coefficients. Futhermore, since each particle is an instance of normal distributions over x_1 and x_2 statistical accuracy for dropout in (x_1,x_2) increases substantially.

SESSION C

Applications

RADIATION TRANSPORT CALCULATION WITHOUT LOCAL THERMODYNAMIC EQULIBRIUM (LTE)

B.A.Voinov, P.D.Gasparyan, Yu.K.Kochubey, V.I.Roslov

The report presents the problem formulation for nonequlibrium radiation transport calculations. The methods for 1-D problems are described. Illustrative test calculations are given.

RADIATION TRANSPORT CALCULATION WITHOUT LOCAL THERMODYNAMIC EQULIBRIUM (LTE)

B.A.Volnov, P.D.Gasparyan, Yu.K.Kochubey, V.I.Roslov

INRODUCTION

The Computational Center of VNIIEF has a variety of methods for various types of radiation transport calculations including multidimensional geometries. The common feature for them is represented by the use of LTE approximation where the source function for photoemission processes is Planck function. However there are some applications where this approximation is not acceptable. These include the calculations of kinetic processes in multicharge ion nonequilibrium plasma typical for a large number of entities encountered in physics of high energy densities /1-6/:

- glow spectra of laboratory plasma obtained in high-performance physical devices (pinch, plasma focus, TOKAM-AK, laser plasma);
- inertial fusion target implosion;
- generation in plasma and X-ray lasers;
- emission spectra of astrophysical objects.

Since experimental studies are complex, expensive and sometimes impossible in laboratory, a method had to be developed to model the objects of this kind and thus to predict and interpret experimental results. This method with its latest version referred to as SS-9 was developed to calculate nonequilibrium radiation transport in one-dimensional geometries.

PROBLEM FORMULATION

The following processes are considered in a radiation collision model:

- spectral transport of photons with source through absorption, emission and scattering reactions;
- kinetics of ion level populations for various chemical compositions and ionization multiplicities including excitation and ionization reactions when ions collide with photons and free electrons;
- two-temperature (T_e,T_i) nonrelativistic gas dynamics with

electron heat conduction included.

Data on interaction between ions, photons and free electrons with a relatively simple ion composition (H, He, Li, , Ne-like ions) is created from calculations of level energies and probabilities for discrete-discrete transitions with relativistic single-electron functions. Cross-sections for photoionization and collision processes are obtained with interpolation formulas /7-9/.

The methods uses the following basic physical approximations:

- complete frequency redistribution approximation for photon absorption/emission processes;
- Maxwell distribution of ions and free electrons over velocity (two-temperature pattern);
- plasma ideality, dense plasma nonideality can be accounted by reducing ionization potentials;
- bright-line radiation absorption cross-sections are assumed to be of Voight type for all transitions except for those in H ions where the impact of plasma microfields on cross-sections and kinetics due to Stark effect can be accounted.

Mathematically, the problem reduces to solving the following equatings in comoving (Lagrangian) frame.

1. Photon transport equation

$$\rho \frac{\partial I_\nu/\rho}{\partial t} + \omega_x \frac{\partial I_\nu}{\partial x} + \hat{L} I_\nu + k(\nu) I_\nu = k_r^*(\nu) B_\nu + k_c(\nu) u_\nu ,$$

where

$I_\nu = I(x,\nu,\vec{\omega},t)$ - radiation intensity, $\vec{\omega}$ - angular variables;

B_ν - Planck function;

$u_\nu = \frac{1}{4\pi} \int I_\nu d\vec{\omega}$ - radiation intensity averaged over angles;

$k(\nu) = k_r(\nu) + k_c(\nu)$ - absorption coefficient;

$k_r(\nu) = k_r(x,\nu,t)$ - total photoabsorption coefficient;

$k_r^*(\nu) = k_r^*(x,\nu,t)$ - total photoemission coefficient;

$k_c(\nu) = k_c(x,\nu,t)$ - Compton-scattering cross-section;

$\hat{L}$ - differencial operator over angular variables;

ρ - gasdynamics material density.

2. Kinetic equations for level populations of material ions

$$\rho \frac{\partial n_i/\rho}{\partial t} + \sum_{i<j} \left(R_{ij} + C_{ij} \right) = \sum_{i>j} \left(R_{ji} + C_{ji} \right) ,$$

where

$n_i = n_i(x,t)$ - level populations ordered with increasing energies;

$R_{ij} = 4\pi \int \frac{d\nu}{\nu} \left(k_{ij}(\nu) u_\nu - k^*_{ij}(\nu) B_\nu \right)$ - radiative disbalance in a transition;

$k_{ij}(\nu) = \sigma_{ij}(\nu) \left(n_i - n_j \frac{n_i^*}{n_j^*} e^{-\frac{\nu}{T_e}} \right)$ - absorption coefficient in a transition;

$k^*_{ij}(\nu) = \sigma_{ij}(\nu)\, n_j \frac{n_i^*}{n_j^*} \left(1 - e^{-\frac{\nu}{T_e}} \right)$ - emission coefficient in a transition;

$\sigma_{ij}(\nu)$ - transition cross-section;

$C_{ij} = n_e c_{ij} \left(n_i - n_j \frac{n_i^*}{n_j^*} \right)$ - collision disbalance;

c_{ij} - collision excitation rate;

$n_i^* = n_i^*(x,t)$ - equlibrium populations obtained for known electron density n_e and temperature T_e.

3. Gasdynamics equations

$$\rho \frac{\partial V}{\partial t} = \frac{1}{x^n} \frac{\partial x^n u}{\partial x} ,$$

$$\rho \frac{\partial u}{\partial t} + \frac{\partial p}{\partial x} = P_r ,$$

$$\rho \left(\frac{\partial}{\partial t} E_e + p_e \frac{\partial}{\partial t} V \right) + \frac{1}{x^n} \frac{\partial}{\partial x} x^n q_e = R_r + Q_{ei} ,$$

$$\rho \left(\frac{\partial}{\partial t} E_i + p_i \frac{\partial}{\partial t} V \right) = -Q_{ei} ,$$

$$\frac{\partial x}{\partial t} = u ,$$

$$V = 1/\rho , \quad p = p_e + p_i ,$$

where

$R_r = 4\pi \int d\nu \left(k_r(\nu)u_\nu - k_r^*(\nu)B_\nu \right)$ - total radiative disbalance;

$P_r = 4\pi \int k(\nu) j_\nu \, d\nu$;

$j_\nu = \frac{1}{4\pi} \int \omega_x I_\nu d\vec{\omega}$ - radiation flux averaged over angles;

$$Q_{ei} = c_{ei} \frac{T_i - T_e}{T_e^{\frac{3}{2}}} ;$$

$$q_e = - \varkappa T_e^{\frac{5}{2}} \frac{\partial T_e}{\partial x} .$$

NUMERICAL METHOD

The transport equation is reduced to quasi-diffusion equations after averaging over angular variables /10/

$$\rho \frac{\partial u_\nu / \rho}{c \partial t} + \frac{1}{x^n} \frac{\partial}{\partial x} x^n j_\nu + k_r(\nu)u_\nu = k_r^*(\nu)B_\nu ,$$

$$\rho \frac{\partial j_\nu / \rho}{c \partial t} + \left(\frac{\partial}{\partial x} D_\nu u_\nu + \frac{C_\nu}{x} u_\nu \right) + k(\nu) j_\nu = 0 ,$$

where D_ν, C_ν - quasi-diffusion coefficients, also referred as Eddington factors. The original transport equation is used to evaluate quasi-diffusion coefficients.

The complete system is computed with the splitting technique. The timestep is divided into two half-steps. One of them solves a system of gasdynamic equations with heat conduction and exchange terms switched off, that is one assumes

$$q_e = P_r = R_r = Q_{ei} = 0,$$

and populations n_i and radiative quantities I_ν, u_ν, j_ν are recomputed from relations of the form

$$\frac{\partial f/\rho}{\partial t} = 0 .$$

A fully conservative difference scheme /11/ is used to compute the

gas dynamics.

The second half-step solves the equations with material motion switched off, that is

$$\frac{\partial V}{\partial t} = \frac{\partial x}{\partial t} = \frac{\partial p}{\partial x} = 0 .$$

Time approximation of equations is performed with a fully implicit first-order accuracy scheme. Quasi-diffusion and electron heat conduction equations are approximated over spatial variables using a second-order integration/interpolation technique. Values for J_ν and q_e fluxes are determined on the cell boundaries while all remaining values are defined in cell centers. The transport equation is approximated over spatial and angular variables using a monotonous nonlinear difference scheme which relies upon the second-order accuracy DS_n-method.

The second half-step is the most difficult to compute. This is due to a high dimension of equations to be solved which actually makes it impossible to use direct methods for solving the system of difference equations. Therefore major efforts were aimed at developing an iteration method based on reduced dimension obtained by efficiently averaging over angular and spectral variables.

The algorithm is as follows. Absorption coefficients and sources for transport and quasi-diffusion equations are computed from a previously obtained population and temperature approximations. Quasi-diffusion coefficients are obtained from transport equation and then used to solve quasi-diffusion equations. Thus found u_ν and J_ν functions are used to solve the remaining equations which complete the first computational stage called simple iteration. The current iteration can be terminated at this point, however it is well known that simple iterations converge too slowly for large optical thickness.

The IF-method /12/ is used for convergence acceleration which can be represented in the simplest way as follows. Let k be the number of a spatial cell, then expressing J_ν by u_ν one obtains the following system for $u_k(\nu) = u(x_k, \nu)$

$$-A^{+}_{k-1}(\nu)u_{k-1}(\nu) + A_k(\nu)u_k(\nu) - A^{-}_{k+1}(\nu)u_{k+1}(\nu) = S_k(\nu) .$$

By introducing unidirectional fluxes

$$j^{\pm}_k(\nu) = A^{\pm}_k(\nu)u_k(\nu) ,$$

we obtain the equations

$$J_k^+(\nu) = R_k^+(\nu)J_{k-1}^+(\nu) + Q_k^-(\nu)J_{k+1}^-(\nu) + W_k^+(\nu)S_k(\nu) ,$$

$$J_k^-(\nu) = Q_k^+(\nu)J_{k-1}^-(\nu) + R_k^-(\nu)J_{k+1}^-(\nu) + W_k^-(\nu)S_k(\nu) ,$$

and an expression is obtained for radiation intensity

$$u_k(\nu) = P_k^+(\nu)J_{k-1}^+(\nu) + P_k^-(\nu)J_{k+1}^-(\nu) + W_k(\nu)S_k(\nu) . \qquad (1)$$

Unidirectional fluxes can be represented as

$$J_k^\pm(\nu) = \pi_k^\pm(\nu)J_k^\pm ,$$

where

$$J_k^\pm = \int J_k^\pm(\nu)\, d\nu, \qquad \pi_k^\pm(\nu) = J_k^\pm(\nu)/J_k^\pm ,$$

and the integration is thought of as a result of applying a quadrature formula used for approximation. The IF-method relies upon assuming unidirectional fluxes to depend slightly on ν, so that the simple iteration evaluates $\pi_k^\pm(\nu)$ in an efficient way.

This assumption results in the following IF implementation which accelerates the simple iteration. Linearize the equations in the vicinity of temperatures and populations from the previous iteration and of intensities from the simple iteration. Correction equations are obtained by taking $\pi_k^\pm(\nu)$ to be known and intagrating over ν

$$\delta J_k^+ = R_k^+\delta J_{k-1}^+ + Q_k^-\delta J_{k+1}^- - \vec{B}_k^+\cdot\delta\vec{n}_k + C_k^+\cdot\delta T_{ek} + D_k^+ ,$$

$$\delta J_k^- = Q_k^+\delta J_{k-1}^+ + R_k^-\delta J_{k+1}^- + \vec{B}_k^-\cdot\delta\vec{n}_k + C_k^-\cdot\delta T_{ek} + D_k^- , \qquad (2)$$

for integral fluxes,

$$-E_{k-1}^+\delta T_{ek-1} + E_k\delta T_{ek} - E_{k+1}^-\delta T_{ek+1} =$$

$$= F_k^+\cdot\delta J_{k-1}^+ + F_k^-\cdot\delta J_{k+1}^- + \vec{F}_k\cdot\delta\vec{n}_k + f_k , \qquad (3)$$

for electron temperature, and

$$\vec{H}_k\cdot\delta\vec{n}_k = \vec{G}_k^+\cdot\delta J_{k-1}^+ + \vec{G}_k^-\cdot\delta J_{k+1}^- + \vec{J}_k\cdot\delta T_{ek} + \vec{\delta}_k .$$

for level kinetics. Relation (1) for intensity and the equation for

ion temperature are used to derive the above equations.

Solving four systems of linear kinetic equations with the same matrices H_k and right-hand sides $\vec{G}_k^+$, $\vec{G}_k^-$, $\vec{G}_k$, $\vec{g}_k$ for each spatial point yields the following representations

$$\delta\vec{n}_k = \vec{h}_k^+ \cdot \delta J_{k-1}^+ + \vec{h}_k^- \cdot \delta J_{k+1}^- + \vec{h}_k \cdot \delta T_{ek} + \vec{N}_k , \qquad (4)$$

which result in a seven-diagonal system for δT_e and $\delta \vec{j}^+$ after substitution into Eqs. (2,3). We find temperature and population values for the current iteration by solving the above system and using relation (4).

NUMERICAL EXAMPLES

1. The well known photon "breakup" /2/ will be exemplified by the following stationary problem. The left side of a fixed plane target is irradiated with isotropic Planck spectrum $B_\nu(T)$, T = 3 Kev, with the dillution factor J_o = 0.01. The right side reflects the radiation. The target of 1cm thick is composed of iron having the density of 0.05 g/cm^3. The computations considered the ground states of H, He, Li-like ions and one excited state of H ion (without accounting the fine structure). The absorption cross-section profile was assumed to be Voight one in the resonance line.

Figure 1 shows the plots for temperature and radiation at the line center. Figure 2 contains the radiation spectrum at the layer boundaries. The dashed curve represents the incident radiation intensity.

The resonance radiation intensity inside the medium increased with a factor of about 50 due to photon "breakup". A similar phenomen (generating resonance radiation in nonequilibrium plasma) is used in laboratory X-ray lasers /5/.

2. Consider the radiation relaxation in unlimited plasma with a constant electron temperature T_e = 2 Kev. The initial radiation intensity is I_ν = 0. Plasma is composed of iron with a density of 0.1 g/cm^3. Excited states of H, He-like ions with the main quantum numbers $n \leq 4$ with level fine structure included and ground state Li ions were considered.

Figure 3 presents the plots for resonance radiation of Ly-α and H ions on the threshold of Lyman continuum as function of time. Figure 4 shows the radiation spectrum at 10 ns. The dashed curve

corresponds to LTE approximation.

For nonequlibrium computations, the plots show the relaxation time to be greater with a factor of about 100 and 10^5 in Lyman continuum and in resonance line, respectively.

3. Multilevel system computations were compared with data reported in literature, in particular with calculations of population inversion in He-like ions of Ba where photopumping was used for the upper level under conditions reported in /13/ - plane target, density of 0.04 g/cm^3, electron temperature of 2 Kev, the excitation rate for upper levels 3^1P_1, 4^1P_1 is about 1 per cent of the radiative decay rate 3^1P_1 -> 1^1S_0, 4^1P_1 -> 1^1S_0.

Figures 5 and 6 present the plots illustrating the relative difference between populations for inversion transitions as a function of optical layer thickness at the resonance line center 1^1S_0 -> 2^1P_1. Note, that collision transition rates had to be changed to improve the agreement between the computational results for the first transition (Fig.5).

CONCLUSIONS

SS-9 is written in FORTRAN preprocessor language, SWIFT, developed by A.Mikiychuk from the Computational Center. The preprocessor capabilities allowed to design a well structured code which is relative easy to tune to specific computer and to FORTRAN dialects and to extend the programming language by introducing the following constructs:

- data structures similar to those of PL/I and C;
- dynamic description of block variables;
- recursive procedures extensively used in routines for initial data evaluation.

A syntax-oriented compiler written in preprocessor language is used for initial data specification, analysis and handling. The total program size is about 30000 FORTRAN statements.

Currently, computations are performed on ELBRUS-2 and IBM PC 286/386.

REFERENCES

1. Zeldovich Ya.B., Raizer Yu.P., Physics of shock waves and high-temperature hydrodynamics phenomena, Moscow, Nauka, 1966

2. Mihalas D., Stellar atmospheres, Moscow, Mir, 1982.
3. Gudzenko L.I., Yakovenko S.I., Plasma lasers, Moscow, Atomizdat, 1978.
4. Duderstadt D., Moses G., Inertial fusion, Moscow, Energoatomizdat, 1984.
5. Elton R.C., X-RAY lasers, San Jiego C.A.: Academic Press, 1990.
6. Plasma theory issues, Moscow, Energoizdat, 1982, no. 12, 1983, no. 13.
7. Sumpson D.H., Astrophys. J. Suppl., 1974, v. 28, 309.
8. Sumpson D.H., Parks A.D., Astrophys. J. Suppl., 1974, v. 28, 323.
9. Moores D.L., Golden L.B., Sumpson D.H., J. Phys., 1980, B.13, 385.
10. Goldin V.Ya., Quasi-diffusion method for the transport equation, J. of Comput. Mat. and Phys., 1964, v.4, no.6, p. 1078-1084.
11. Samarsky A.A., Popov Yu.P., Difference methods for calculations in gas dynamics, Moscow, Nauka, 1980.
12. Kochubey Yu.K., IF-method for one-dimensional nonequilibrium radiation transport calculations, VANT, Ser.: Met. and Progr. for Num. Calcul. in Comput. Phys., 1988, no.1, p.46-56.
13. Alley G.E., Chapline G., Kunasz P., Weisheit J.C., Calculation of gain at X-ray wavelengths resulting from optical pumping of helium-like ions. JQSRT, 1982, v. 27, 257.

SESSION C

Applications

Mathematical Modeling of Flexible Plastics and Destruction of Materials.
Seismic Decoupling of an Underground Nuclear Explosion.
Vladimir Bychendov, Valentin Kuropatenko, et al. (Chelyabinsk)

MATHEMATICAL MODELLING OF FLEXIBLE PLASTICS AND DESTRUCTION OF MATERIALS. SEISMIC DECOUPLING OF AN UNDERGROUND NUCLEAR EXPLOSION

V.A. Bychenkov, A.A. Gorno..., V.F. Kuropatenko

A continuous medium is examined as a combination of matter and voids:

$$V = V_m + \theta$$

where V is the specific volume of the medium, V_m is the specific volume of material (solid and liquid components), θ is the specific volume of [illegible] (void, gases), and $\Psi = \theta/V$ is the porosity.

One of the determining functions of the model is the equation of state of the material

$$P_m = f(V_m, E_m)$$

where E_m is the specific internal energy after subtraction of work [illegible] of stresses on flexible shears, P_m is the average pressure on the material. The mass and pressure of gas in the pores are neglected The average stresses on the medium σ_{ij} and on the substance $\sigma^{(m)}_{ij}$ are associated with the ratios:

$$\sigma_{ij} = \sigma^{(m)}_{ij}(1-\Psi)$$

$$\sigma_{ij} = -P\delta_{ij} + S_{ij} \quad ,$$

where S_{ij} is the deviator of the tensor of stresses,

δ_{ij} is the symbol of Kronecker

The law of deformation of porous medium is based on the relation of pressure to porosity for a given irreversible selection of pores.

$$P = P_{cr}\exp\left(\frac{\Psi}{\Psi_o}\ln\frac{P_e}{P_{cr}}\right), \qquad (1)$$

where Ψ_o is the initial porosity, $P_e = P_e(\Psi_o)$ is the vapor pressure, P_{cr} is the pressure of pores closing. The law (1) was proposed by

Butkovich [1] for approximation of data on various rocks and is the limit function $P(\Psi)$. In general, as the determining correlation of a porous medium, we use the equation

$$\frac{d\ln V_m}{d\ln V} = F(\Psi, V, P), \qquad (2)$$

while the functions $F(\Psi, V, P)$ are different for charging and discharging. In particular, equations (1) corresponds to

$$F = Fp = \frac{P(1+C)}{P(1+C)-KsVm},$$

where Ks is the modulus of volume expansion of material, $C = 1/\Psi_o \ln Pe/P_{cr}$. Discharging and plastic charging of porous material is described by the function:

$$F = Fe(\Psi) > F_p(\Psi, V, P).$$

$Fe(0) = 1$, $Fe(\Psi) = 0$ when $\Psi \geq \Psi_{oo}$

where Ψ_{oo} is the maximum porosity. The value $F = 1$ in equation 2 corresponds to non-porous medium given the non-fulfillment of additional friability conditions.

A stable medium loses stability at a fracture point when there is extension and displacement, when the extent of accumulated damages ω reaches the value 1. The formation and development of fissures and the formation of cleavage from the action of elongating stresses is described within the framework of a statistical thermo-fluctuational model of the kinetics of cleavage [2]. The extent of breakage ω is increased over the course of time t as a function of maximum stress $\sigma > 0$:

$$\frac{d\omega}{dt} = \frac{1}{t\sigma}, \qquad (3)$$

where

$$t\sigma = t_o \exp\{\frac{T_o}{T}[\sigma - (\frac{C_e t_o}{U_a^{1/3}})^{3\beta\sigma} \frac{\sigma}{K_s + 4/3\,\mu}]\}. \qquad (4)$$

t_o is the period of thermal vibrations of atoms, $\varepsilon\sigma$ - 0.2, C_e is the velocity of longitudinal waves, U_a is the volume of an atom, $T_o = C_p/\alpha R$, α is the coefficient of linear expansion, R is the gas constant, T is the temperature, $\beta\sigma$ is the coefficient of homogeneity, C_p is the specific heat capacity, μ is the shear modulus. Model (3)-(4) was obtained on the basis of the Arrenius equation incorporating statistical concepts concerning structural defects of the material in the form of a Weibull distribution function. When ω reaches the value of 1, the solid medium converts to fractured. The fractured medium is described either as isotropic or as anisotropic. Friability and compaction of a fractured medium is described by the equation:

$$\frac{d\Psi}{dt} = \frac{1-\Psi}{3K_s}(1+\nu)\cdot\frac{\delta_1\overset{\nabla}{\sigma}_1 + \delta_2\overset{\nabla}{\sigma}_2 + \delta_3\overset{\nabla}{\sigma}_3}{1+\nu(\delta_1+\delta_2+\delta_3-2)} \qquad (5)$$

where ν is Poisson's ratio, $\overset{\nabla}{\sigma}_1$ is Yaumanov's derivative from the main stresses under conditions of flexible deformation, $\delta_i = 0$, where i corresponds to the "stable" direction and $\delta_i = 1$, if i corresponds to the "unstable" direction. The isotropic fractured medium with open fissures is characterized by values of $\delta_i = 1$ in (5) in all directions i = 1,2,3. Conditions of closing fissures: $\Psi = \Psi_o$. Friability of fractured medium at the moment of destruction is described by an analog of equation (5) in terms of increments. Destruction on shear of a friable medium is associated with reaching tangential stresses of boundary values

$$T = 3/2\ S_{ij}\ S_{ij} = Y(\Psi, V, P),$$

where Y is the effective dynamic value of the yield point. The medium fractured on shear can be fractured by the action of shear deformation (dilation effect) according to law (5) with

$$\delta_i = \begin{cases} 0, & \sigma_i < 0 \quad \text{or} \quad \overset{\circ}{\sigma}_i \leq 0 \\ 1, & \sigma_i = 0, \ \overset{\circ}{\sigma}_i > 0 \end{cases}$$

The change in shear stresses in the medium is modelled both within the framework of the associated law as well as taking into account the relaxation of stresses and obeys the equations:

$$\frac{dS_{ij}}{dt} + \lambda \cdot S_{ij} = 2\mu \dot{e}_{ij} + \Omega_{ik} S_{kj} + \Omega_{jk} S_{ki}, \qquad (6)$$

where $\dot{e}_{ij}$ is the deviator of tensor velocity of deformation $\dot{\varepsilon}_{ij}$,

$$\dot{\varepsilon}_{ij} = \frac{1}{2}\left(\frac{\partial U_i}{\partial x_j} + \frac{\partial U_j}{\partial x_i}\right), \quad \Omega_{ij} = \frac{1}{2}\left(\frac{\partial U_i}{\partial x_j} - \frac{\partial U_j}{\partial x_i}\right)$$

is the rotation tensor, U_i is the vector of mass velocity. When using the associated law of flow, the dissipative function $\lambda \geq 0$ in (6) is determined from the correlation

$$\lambda = \begin{cases} \frac{3\mu}{Y^2} S_{ij} \dot{e}_{ij} - \frac{\partial \ln Y}{\partial t}, & S_{ij} S_{ij} = \frac{2}{3} Y^2 \\ 0, & S_{ij} S_{ij} < \frac{2}{3} Y^2 \end{cases} \qquad (7)$$

Calculation of the relaxation of stresses proceeds on the basis of statistical thermo-fluctuational theory [3]. According to this the function λ in (6) is defined as:

$$\lambda = \begin{cases} \left(1 - \frac{Y}{J}\right) \frac{1}{t_s}, & J > Y \\ 0, & J \leq Y, \end{cases} \qquad (8)$$

Relaxation time t_s in (8) is determined from the equation

$$t_s = t_0 \exp\left\{\frac{T_0}{T}\left[s - \rho_{ok}V - \left(\frac{C_e t_s}{U_a^{1/3}}\right)^{3\varepsilon_s} \frac{-Y}{2\mu}\right]\right\}. \qquad (9)$$

where $\varepsilon_s \sim 1.2$, ρ_{ok} is the crystalline density. In the absence of movement the intensity of shear stresses T decreases over time t according to a law similar to law (9), if we place $t_s \equiv t$ in (9). Equations (6) and (8) with $Y \equiv 0$ correspond to Maxwell's model of relaxation of stresses. Introduction of $Y > 0$ into (9) is equivalent to disregarding the relaxation of small stresses, when the relaxation time turns out to be much greater than the characteristic time of the problem and enables us to improve the economy of the numerical method.

Equations (6) with function λ in the form of (8) enable us to assure fulfillment of hyperbolic conditions for a complete system of differential equations. The conditions of thermodynamic correctness of the model are fulfilled as a consequence of deducting the percentage of E_s from the specific internal energy in the equation of state:

$$\frac{dE_s}{dt} = \frac{V}{2\mu} S_{ij} \frac{dS_{ij}}{dt}.$$

Equations of associated law (6) with λ in the form of (7) lead [4] to a disruption of the hyperbolic conditions for equations of plastic flow for a number of stressed states on the surface of flow $J = Y$.

Dynamics problems of flexible plastic deformation of materials under conditions of explosive charge are solved with the aid of the explicit two-dimensional Lagrangian differential method [5,6]. The method is aimed at solving dynamics problems in adiabatic approximation by isolating contact boundaries and using artificial viscosity to calculate the movement of shock waves. Artificial viscosity contains linear and quadratic terms and is introduced in

the presence of compression ($\partial u/\partial x < 0$) of a grid interval. In a weak wave viscosity is introduced, if $\partial u/\partial x < 0$, $\partial^3 u/\partial x^3 > 0$. In the first moment an independently regular quadrangular grid is constructed in each area of the system. In the process of calculating, a regular grid can be locally replaced by an irregular quadrangular grid. In light of this, joining of a number of neighboring units takes place; however, regular structure of grid data of a matrix type is preserved. If thermodynamic parameters of neighboring joined units differ qualitatively, then evolution is traced within the framework of the adiabatic mechanically quasi-equilibrium mixture. A grid of Dirichlet (Voronyi) units formed around Lagrangian free points can be placed in conformity to areas with an irregular quadrangular grid.

As a whole, the mathematical model correlates the methods of M. L. Wilkins, George Mainchek and S. Sak [7].

Figures 1-4 present the results of calculations of seismic decoupling of an underground nuclear explosion in granite, water-saturated tuff, rock salt and alluvium. Relaxation of stresses in the rock were not accounted for, but the decreased value of flow boundary was ascribed to fractured material. Air and graphite were the energy absorbents. Equation of state of the air was used in tabular form [8], equation of state of graphite and rocks was constructed accounting for evaporation [9]. Calculations were done in unidimensional approximation accounting for a pressure of 30 bars. The first stage of calculations of an underground nuclear explosion in air chambers was carried out in hydrodynamic approximation - the pressure in the trajectory near the chamber and outside the action of the heat wave was determined. The characteristics of the rocks and the graphite used in the calculations are presented in Table 1.

Table 1

Characteristics of Materials

(ρ is density, Z is mass concentration of water, Y_o is linking of stable media, Y_* is max Y(P) for fractured media, Q_{sub} is the heat of sublimation)

HP	ρ, g/cm^3	Z	Ψ_o	Ce, km/c	Y_o, GPa	Y_*, GPa	Q_{sub}, kdzh/z
1. Granite	2.61	0	0.012	5.5	0.2	0.2	20
2. Salt	2.25	0	0	4.55	0.1	0.015	7
3. Tuff	1.98	0.124	0	2.71	0.025	0.05	10
4. Alluvium	1.8	0.23	0.035	1.71	0.005	0.03	10
5. Graphite	0.5÷1	0	0.78÷ 0.56		0	0	60

Figure 1 shows the function $\zeta(\Gamma_p)$, where Γ_p is the radius of the air chamber, ζ is the ratio of maximum value of spherical corrected potential in reference calculation with a dense obstruction to the corresponding value in calculation with the chamber. Functions $\zeta(\Gamma_p)$ of the underground nuclear explosion in air chambers are non-monotonic. The lower the stability of the rock, the higher the value of minimal radius of the chamber $\Gamma_\flat$, weakening the seismic effect (SE). Calculated values Γ [m/kt$^{1/3}$] turned out to be equal: 6.2 (for underground nuclear explosion in granite); 8.5 (salt); 9.7 (tuff); and 15.5 (alluvium). Given a radius of the chamber, $\Gamma_p < \Gamma_\flat$ anti-decoupling takes place. The higher the [illegible] degree of weakening of SE, the higher the stability of the rock.

Increasing the porosity of the medium in the area surrounding the blast facilitates lowering the SE. When the initial porosity is low, less filled, ($\Psi \leq 0.4$), the decrease of the SE depending on the radius of the porous area is a monotonic function. If the porosity is high, then this function becomes non-monotonic, intensification of the SE of the underground nuclear

explosion corresponds to small radii $\Gamma_p < \Gamma_b$ (Ψ_o). Given $\Gamma_p > \Gamma_b$ (Ψ_o) the SE diminishes more quickly, the higher the value of Ψ_o. The value of Γ_b (Ψ_o) increases with the growth in Ψ_o; at the boundary, the function $\zeta(\Gamma_p$ yields to the function $\zeta(\Gamma_p)$ for air chambers.

For each radius of the chamber there is a corresponding value of porosity which diminishes the SE of the underground nuclear explosion the most effectively. A further increase in effectiveness of energy absorption is associated with the substitution of porous containing medium for material having a high value of sublimation energy. Figures 2 and 3 show the functions of (Γ_p) of an underground nuclear explosion in graphite chambers given values of graphite density of 0.5 and 1 g/cm^3, respectively. Analysis of the results of calculations of the underground nuclear explosion in homogeneous graphite and air chambers demonstrate that the dependence of optimal density of energy absorbent on radius of chamber of the underground nuclear explosion in tuff can be expressed by the following approximate formula:

$$\rho \approx \rho_{ok} \cdot 2^{1-\Gamma p/\Gamma o}$$

where $\rho_{ok} = 2$ g/cm^3, $\Gamma_o = 2$ m/kt$^{1/3}$.

The effectiveness of the energy absorbent can be significantly increased by means of lowering its density with the growth of Γ. Figure 4 shows the function $\zeta(\Gamma_p)$ of the underground nuclear explosion in tuff using different types of energy absorbent media. Using combined energy absorbent (graphite, density $\gtrsim 2$ g/cm^3 for $\Gamma \leq 2$ m/kt$^{1/3}$ + air) enables the weakening of the SE of the underground nuclear explosion in a chamber with a radius of 10 m/kt$^{1/3}$ by more than 4 times. Given this fact, the average density of energy absorbing medium turns out to be equal to 0.02 g/cm^3, but the mass of graphite is lowered by several times in comparison with the mass corresponding to homogeneous distribution of graphite of optimal density.

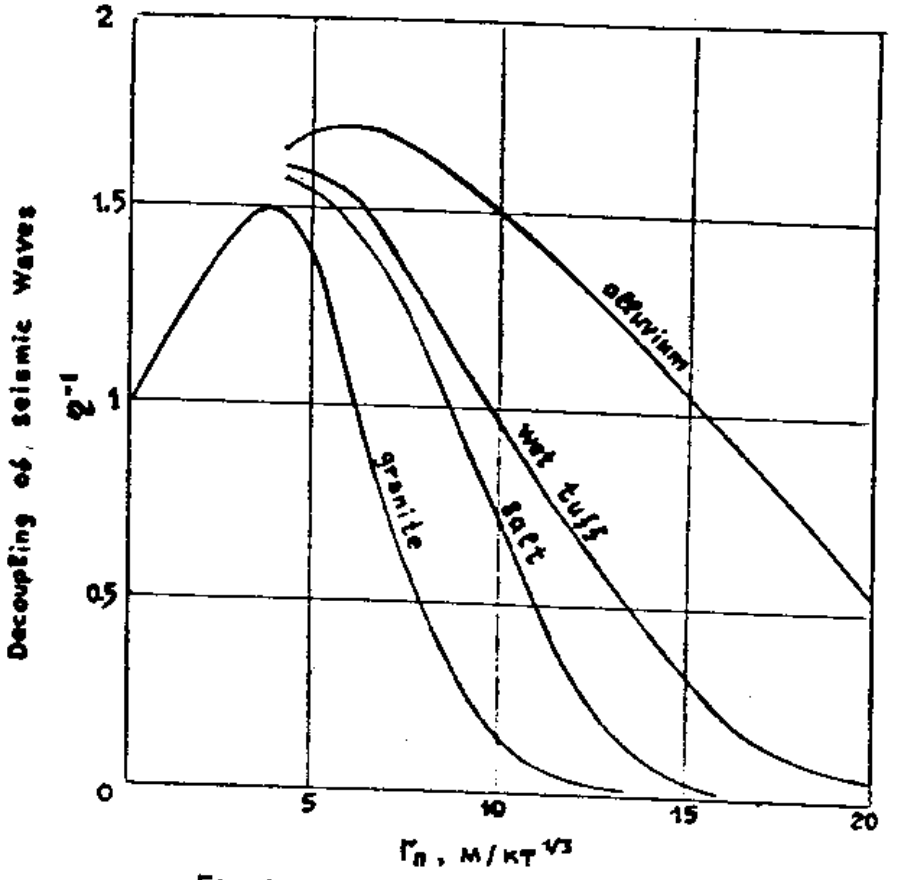

Fig. 1. Air Cavity

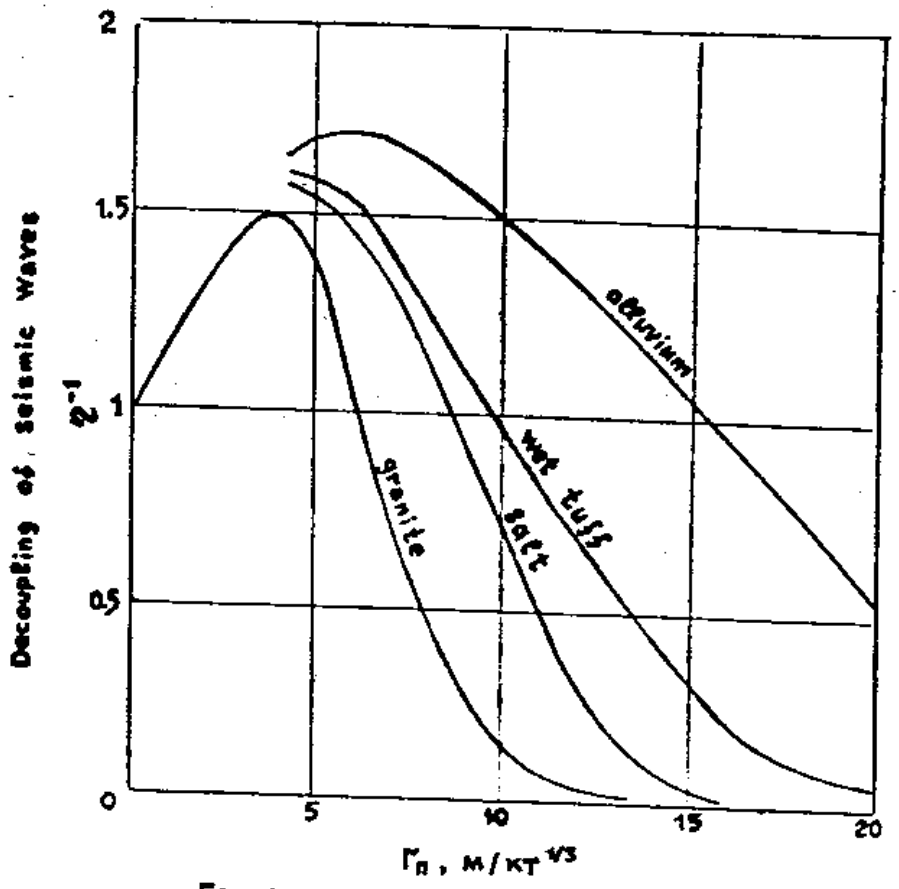

Fig. 1. Air Cavity

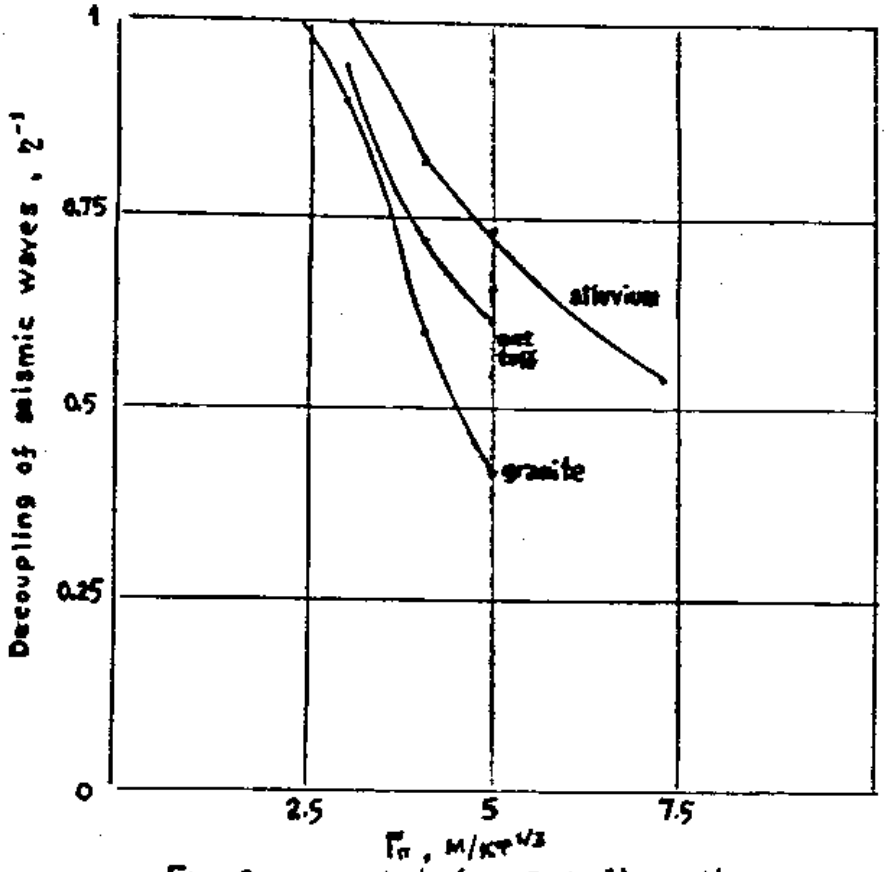

Fig. 2. graphit (ρ=a5g/cm^3) cavity

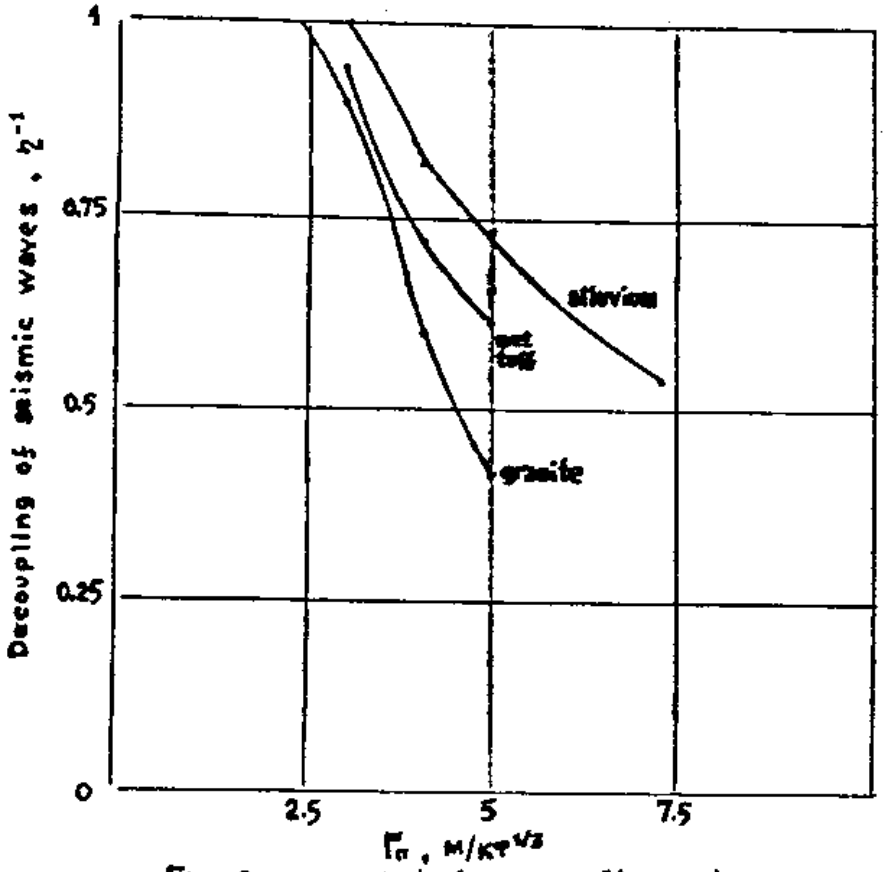

Fig. 2. graphit ($\rho = 2.5 g/cm^3$) cavity

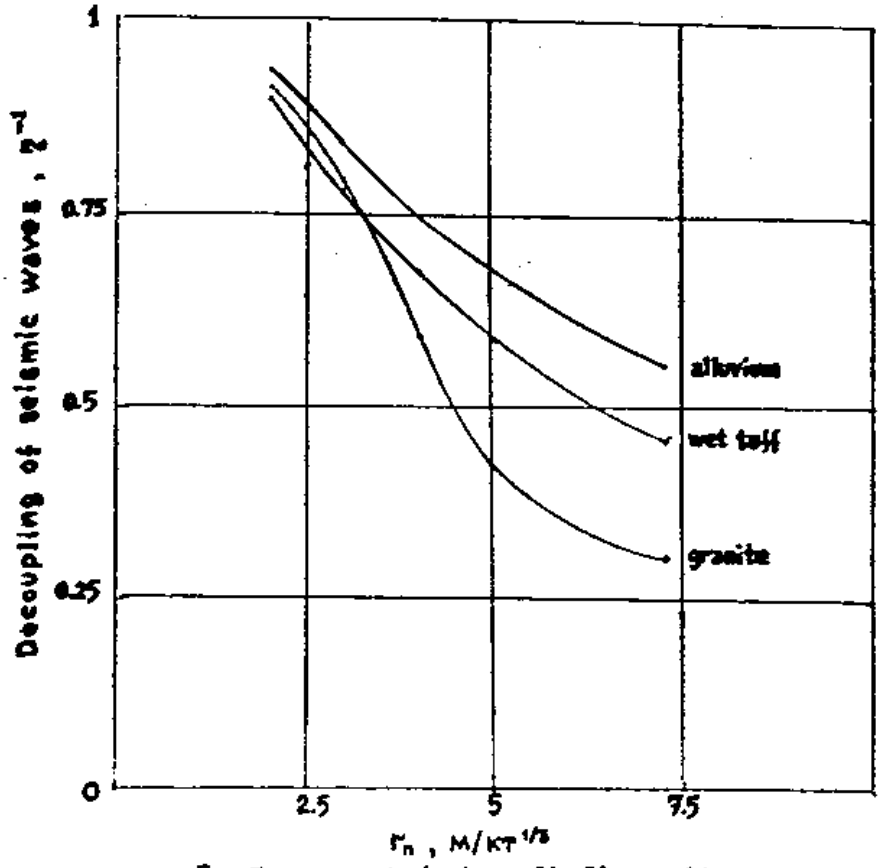

Fig.3. graphit ($\rho = 1\ g/cm^3$) cavity

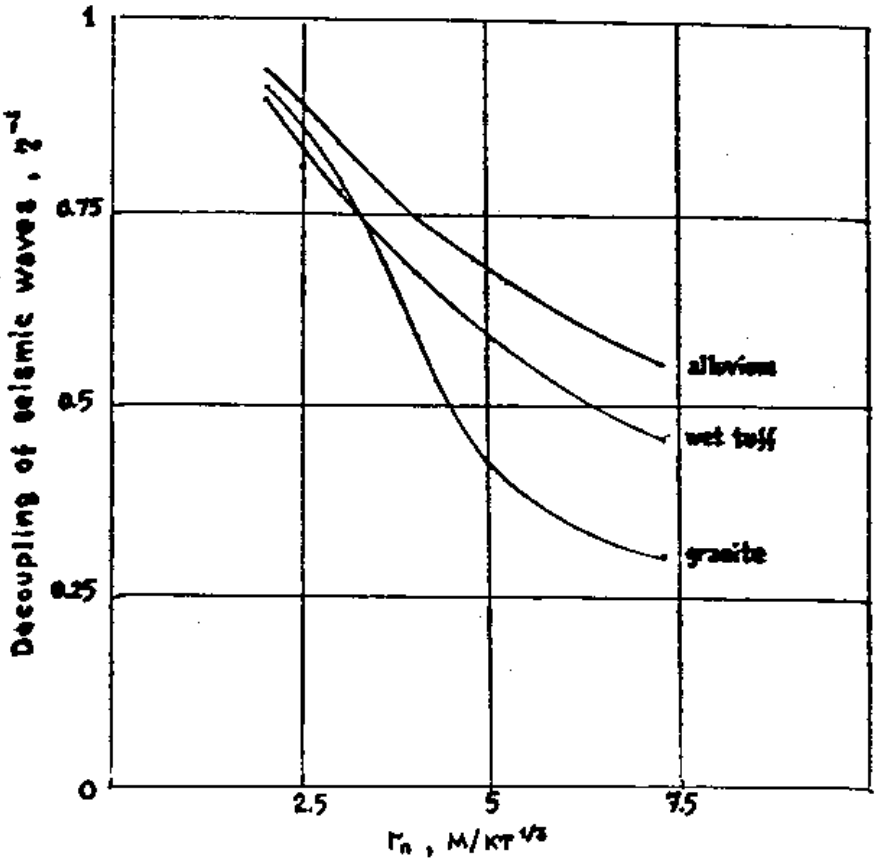

Fig.3. graphit (ρ=1 g/cm³) cavity

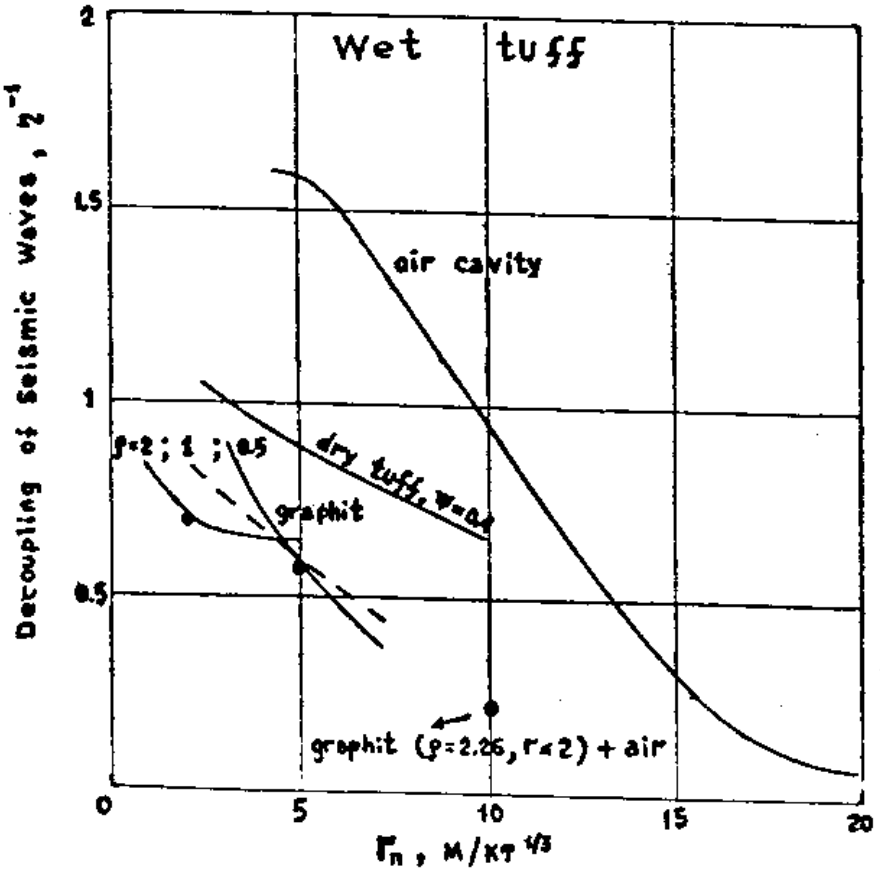
Wet tuff
air cavity
dry tuff, W=0.2
ρ=2 ; 1 ; 0.5
graphit
graphit (ρ=2.26, r<2) + air
Decoupling of Seismic Waves, r⁻¹
Rn, M/KT^1/3
0
5
10
15
20
0.5
1
1.5
2
Fig. 4

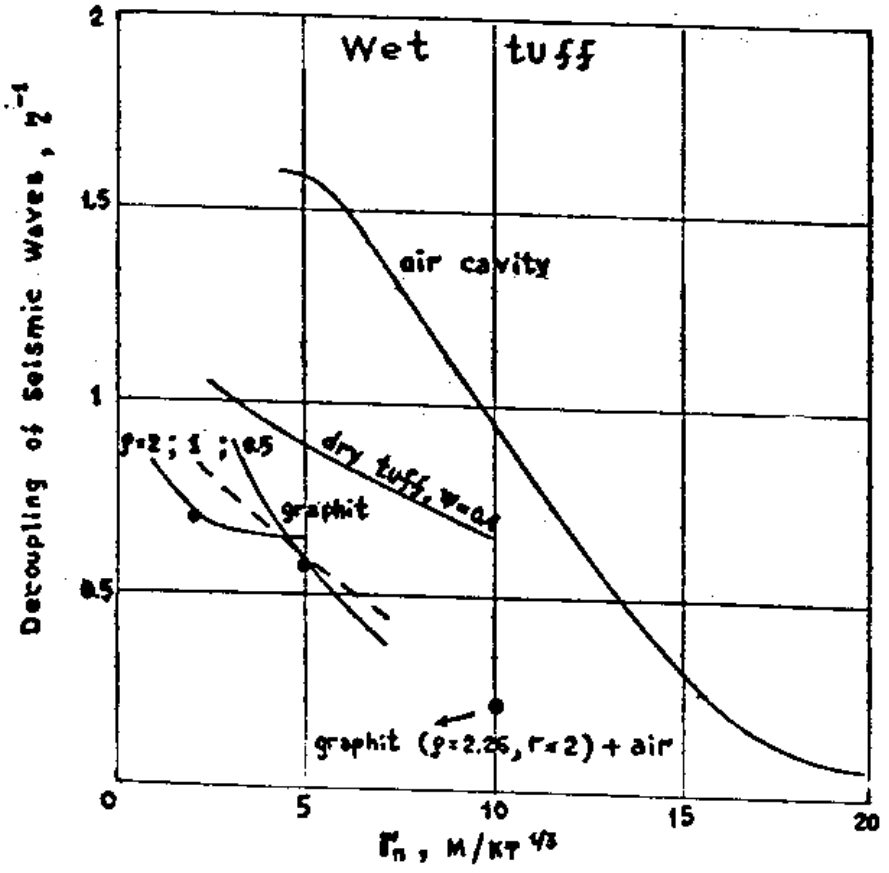
Wet tuff
air cavity
dry tuff, W=0.
ρ=2; 1; 0.5
graphit
graphit (ρ=2.26, r=2) + air
Decoupling of Seismic Waves, r⁻¹
r̄n, M/KT^1/3
0
5
10
15
20
0.5
1
1.5
2
Fig. 4

Literature

1. Butkovich, T.R. A Technique for Generating Pressure-Volume Relationship and Failure Envelopes for Rocks. Lawrence Livermore Laboratory, UCRL-51441, 1973.

2. Sanin, I.V., Vorobev, A.I., Gornovoi, A... Kinetic, statistical model of splitting destruction of metals. FGV, No. 1, 1987, pp. 67-70.

3. Gornovoi, A.A., Kozlov, E.A., Muzyrya, A.K. Shorokhov, E.V. Research in the kinetics of relaxation of flexible indication in steel 3 and titanium. FGV, No. 1, 1989, pp. 142-144.

4. Bychenkov, V.A., Svidinskii, V.A. Incorrectness of model of flexible plastic flow in Wilkins' method. FGV, No. 1, 1990, pp. 118-122.

5. Bychenkov, V.A., Gadzhieva, V.V. "Octopus" method of calculation of two-dimensional turbulent flows of destroyed media. Issues [illegible] of science and technology, Ser. "Methods and programs of [illegible] solution of problems of mathematical physics," . 2(2), 1978, pp. 12-22.

6. Alekseeva, T.N., Bychenkov, V.A., Kuropatenko, V.F. RAPID method of calculating two-dimensional adiabatic flows of compressible media in Lagrangian variables with free proximity [illegible]. Ibid., . 1, 1988, pp. 14-21.

7. Methods in computational physics Advances in Research and Applications. Vol. 3, Fundamental Methods in Hydrodynamics. Academic Press: New York and London, 1964.

8. Kuznetsov, N.N. Thermodynamic functions and shock adiabats of air at high temperatures. Moscow: Machine building, [illegible

date].

9. Kuropatenko, V.F., Minaeva, I.S. Mathematical model of equation of state of quartz. VANT, Ser. "Mathematical modelling of physical processes," . 1, 1989, pp. 75-76.